Indian Journal of Chemical Technology
Vol. 31, March 2024, pp. 186-196
DOI: 10.56042/ijct.v31i2.5482

Influence of Ohmic heating and thermal radiation on chemically reactive pulsatile flow of Casson nanofluid in a vertical porous channel embedded in non-Darcy porous medium

A. Subramanyam Reddy[1], Kalyan Kumar Challa[2]*, S. Srinivas[3], T.R. Ramamohan[4] & K. Vajravelu[5]

[1]Department of Mathematics, School of Advanced Sciences, Vellore Institute of Technology, Vellore-632 014, Tamil Nadu, India

[2]Department of Mathematics, Narayana Engineering College (Autonomous), Gudur, Tirupati-524 101, India

[3]Department of Mathematics, School of Advanced Sciences, VIT-AP University, Inavolu, Vijayawada – 522 237, India

[4]Department of Chemical Engineering, M S Ramaiah Institute of Technology, Bangalore-560 054, India

[5]Department of Mathematics, University of Central Florida, Orlando, FL 32816, USA

*E-mail: kalyankumar.challa@gmail.com

Received 10 September 2023; accepted 29 January 2024

The present study examines the effects of the pulsatory flow of Casson nanofluid using Buongiorno's model in a vertical channel. On the left wall, fluid is injected with some velocity and removed at the opposite wall at the same rate. The solutions for velocity, temperature, nanoparticle concentration, heat, and mass transfer rates are calculated using the Runge-Kutta 4th order approach along with the Shooting method. The impact of different parameters, including thermophoresis, chemical reaction, Lewis number, and heat source or sink parameter, are illustrated graphically. The results show that the Brownian motion parameter increases the temperature profile, while the chemical reaction parameter decreases the concentration profile. Further, a tabular representation of the steady and unsteady heat and mass transfer rates at the left wall is provided. The higher values of the chemical reaction parameter result in an increase in both the steady and unsteady Sherwood number distributions.

Keywords: Casson nanofluid, Chemical reaction, MHD, Pulsatile flow, Thermal radiation

Introduction

Nanofluids are different types of fluid made up of convectional base liquids and nanometre-sized particles. Nanofluid research is a significant scientific field because of the wide range of potential applications in mineral oil, water, solar energy, and microelectronics. In chemotherapy, nanoparticles are also utilised to kill cancer cells. Applications of nanofluids in technology and engineering include cancer therapeutics, vehicle thermal management, nuclear systems cooling, intensified microreactors, electronic cooling components, and many more[1-10]. Buongiorno[11] created a nanofluid model by submerging nanoparticles in a base fluid and concluded that the nanofluid had higher thermal conductivity and single-phase heat transfer than the base fluid. He continued by saying that the improvement in heat transfer coefficient outweighs the influence of pure thermal conductivity. Ghasemi *et al.*[12] examined the peristaltic flow of nanofluids in drug delivery systems. Investigation of MHD Casson nanofluid flow across an inclined porous stretching surface was performed by Ghadikolaei *et al.*[13] Electro-osmotic transportation of nanofluid in a channel has been inquired by Das *et al.*[14]. Farooq *et al.*[15] scrutinized the impacts of a two-dimensional stream of Casson nanofluid across plate/cylinder including bioconvection, motile microorganisms, exponential thermal source/sink, and non-linear thermal radiation.

There have been many studies on pulsatory flows in channels and pipes[16-21]. Still, very few studies on non-Newtonian nanofluid flow with pulsating pressure gradients have been documented in the literature. Dusty liquid flow in a channel has been inquired by Datta *et al.*[22] Rana & Murthy[23] demonstrated the analysis of pulsation non-Newtonian fluid flow in a tube. Shit *et al.*[24] numerically investigated the pulsatory blood flow through a porous overlapping constricted artery. In a vertical channel, pulsatile Casson nanofluid flow was examined by Kumar *et al.*[25] using Buongiorno's model. Vasu *et al.*[26] studied the micropolar pulsatory blood flow through a diseased tapered artery. Kumar and Srinivas[27] have examined the pulsation Casson fluid flow in a

vertical channel. Ali *et al.*[28] numerically investigated the pulsatory Casson fluid flow through a double-constricted channel. The pulsatory flow of nanofluid with heat transfer in a permeable channel is discussed by Govindarajulu and Reddy[29]. Wang *et al.*[30] demonstrated the pulsatory blood flow pass a small vessel under a magnetic field. Srinivas *et al.*[31] has investigated the cross-diffusion effects of pulsation Casson fluid flow in a vertical permeable channel. There are numerous significant technical issues concern the flow of chemically reacting fluid mixtures. Many biological fluid systems are examples of such mixtures. For example, blood is a complex mixture of plasma, proteins, cells, and a variety of other chemicals that is modelled usually in a homogenized sense as a single constituent fluid. Blood is an example of a Casson fluid.

The study of heat and mass transfer problems with chemical reactions are of great importance in many applications such as polymer production, drying, distribution of temperature and moisture over agricultural fields and groves of fruit trees, damage of crops due to freezing, evaporation at the surface of a water body and energy transfer in a wet cooling tower and flow in a desert cooler[32-37]. Rauf *et al.*[38] explored the Casson nanofluid's three-dimensional boundary layer flow in the presence of a chemical reaction. Raju *et al.*[39] numerically examined the chemical reaction and heat source behaviour of Casson fluid towards the stretching surface. Combined influences of chemical reaction and radiation absorption onto the unsteady hydromagnetic Casson fluid flow through an infinite inclined absorbent plate was examined by Swarnalathamma *et al.*[40]. Asogwa *et al.*[41] demonstrated the radiative characteristics of EMHD Casson nanofluid over a stretchable electromagnetic plate. Yousef *et al.*[42] reported on hydromagnetic Casson-Williamson nanofluid flow through a slippery stretching sheet under the impact of a chemical reaction. Devi & Srinivas[43] demonstrated the combined impacts of chemical reaction and heat source on the flow of two-layered viscoelastic liquids in a vertical porous channel. Very recently, Srinivas *et al.*[44] investigated the hydromagnetic flow of a Powell-Eyring nanofluid with the oscillatory pressure gradient through the horizontal channel under the impact of a chemical reaction.

The primary goal of this work is to study the numerical analysis of hydromagnetic Casson nanofluid using Buongiorno's model in a vertical porous channel generated by a pulsating pressure gradient.

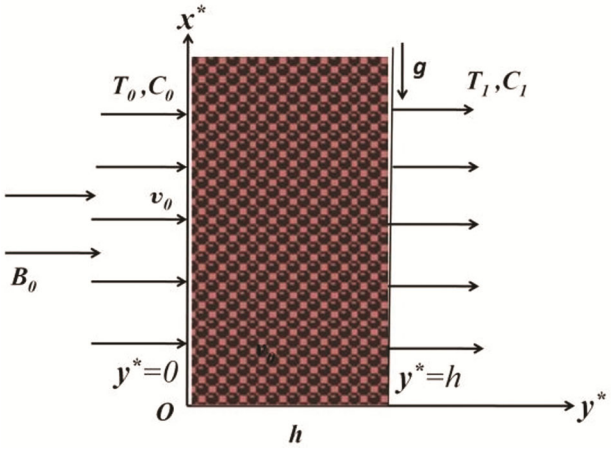

Fig. 1 — Flow model of the problem

Modelling and formulation

Consider a fully developed laminar pulsatory flow of an electrically conducting Casson nanofluid between two parallel walls separated by a distance h. On the left wall, fluid is injected with a velocity v_0 and removed at the opposite wall at the samerate. A uniformly strength magnetic field B_0 is applied orthogonal to the walls (see Fig. 1). Here T_0, C_0 represents the temperature and concentration at the left wall, while the uniform temperature and concentration, T_1, C_1, are considered on the right wall. The rheological equation of the non-Newtonian Casson fluid model is defined as

$$\tau_{ij} = \begin{cases} 2(\mu_B + P_{y^*}/\sqrt{2\pi_c})e_{ij}, & \pi_c > \pi \\ 2(\mu_B + P_{y^*}/\sqrt{2\pi})e_{ij}, & \pi > \pi_c \end{cases} \quad \ldots(1)$$

The governing equations are

$$\frac{\partial u^*}{\partial t^*} + v_0 \frac{\partial u^*}{\partial y^*} = -\frac{1}{\rho_f}\frac{\partial P^*}{\partial x^*} + \nu_f\left(1+\frac{1}{\beta}\right)\left(\frac{\partial^2 u^*}{\partial y^{*2}}\right) + g\beta_T^*(T^*-T_0) + g\beta_C^*(C^*-C_0) - \frac{\sigma_f B_0^2}{\rho_f}u^* - \frac{\mu_f \Phi}{\rho_f k}u^* - \frac{C_b}{\sqrt{k}}u^{*2} \quad \ldots(2)$$

$$\frac{\partial T^*}{\partial t^*} + v_0\frac{\partial T^*}{\partial y^*} = \frac{k_f}{(\rho C_p)_f}\frac{\partial^2 T^*}{\partial y^{*2}} + \tau D_B\left(\frac{\partial C^*}{\partial y^*}\frac{\partial T^*}{\partial y^*}\right) + \tau\frac{D_T}{T_m}\left(\frac{\partial T^*}{\partial y^*}\right)^2 + \frac{\mu_f}{(\rho C_p)_f}\left(1+\frac{1}{\beta}\right)\left(\frac{\partial u^*}{\partial y^*}\right)^2 - \frac{1}{(\rho C_p)_f}\frac{\partial q_r^*}{\partial y^*} + \frac{\sigma_f B_0^{\,2}}{(\rho C_p)_f}u^{*2} + \frac{Q_0}{(\rho C_p)_f}(T^*-T_0) \quad \ldots(3)$$

$$\frac{\partial C^*}{\partial t^*}+v_0\frac{\partial C^*}{\partial y^*}=D_B\frac{\partial^2 C^*}{\partial y^{*2}}+\frac{D_T}{T_m}\left(\frac{\partial^2 T^*}{\partial y^{*2}}\right)-k_1C^* \quad ...(4)$$

subject to the boundary conditions

$$u^*(0)=0,\ T^*(0)=T_0,\ C^*(0)=C_0;\ u^*(h)=0,\ T^*(h)=T_1,\ C^*(h)=C_1 \quad ...(5)$$

where Q_0 indicates the heat source (or sink), μ_f is the dynamic viscosity, T_m is mean temperature, κ_f is the thermal conductivity, e_{ij} is the $(i,j)^{th}$ component of the strain rate tensor, $(\rho C_p)_p$ is the effective heat capacity of the nanoparticles, $\pi=e_{ij}^2$ denotes the product of the component of the strain rate tensor, p^* is dimensional pressure, D_T is thermophoretic diffusion coefficient, π_c is the critical value of this product based on the non-Newtonian fluid, ν_f is the kinematic viscosity, P_{y^*} is the yield stress of the fluid, σ_f is electrical conductivity, μ_B is the plastic dynamic viscosity of the non-Newtonian fluid, D_B is Brownian diffusion coefficient, τ_{ij} is the $(i,j)^{th}$ component of the stress tensor, T^*, C^* represent the dimensional temperature and concentration of the fluid, $(\rho C_p)_f$ is the heat capacitance of nanofluid, $\tau=(\rho C_p)_p/(\rho C_p)_f$, C_b is the form of drag coefficient, β_C^* is the coefficient of concentration expansion, g is the acceleration due to gravity, $\beta=\frac{\mu_B\sqrt{2\pi_c}}{P_{y^*}}$ is Casson fluid parameter, β_T^* is the coefficient of thermal expansion, Φ and k are the porosity and permeability of porous medium, t^* is time, ρ_f is density of the fluid, u^* is dimensional velocity in x^* direction and k_1 is 1st order chemical reaction rate($k_1<0$ for generative reaction, $k_1>0$ for destructive reaction, $k_1=0$ for no reaction). The radiative heat flux, on using Rosseland approximation, reduces to

$$q_r=-\frac{4}{3}\left(\frac{\partial T^{*4}}{\partial y^*}\right)\frac{\sigma^*}{\chi} \quad ...(6)$$

where, χ represents the coefficient of Rosseland mean absorption, the Stefan-Boltzmann constant represented by σ^* and $T^{*4}\cong 4T_0^3T^*-3T_0^4$. Therefore, Eq. (3) becomes

$$\frac{\partial T^*}{\partial t^*}+v_0\frac{\partial T^*}{\partial y^*}=\frac{\kappa_f}{(\rho C_p)_f}\frac{\partial^2 T^*}{\partial y^{*2}}+\frac{\mu_f}{(\rho C_p)_f}\left(1+\frac{1}{\beta}\right)\left(\frac{\partial u^*}{\partial y^*}\right)^2+\frac{1}{(\rho C_p)_f}\frac{16\sigma^*T_0^3}{3\chi}\frac{\partial^2 T^*}{\partial y^{*2}}+\frac{\sigma_f B_0^2}{(\rho C_p)_f}u^{*2}+\frac{Q_0}{(\rho C_p)_f}(T^*-T_0)+\tau\left[D_B\left(\frac{\partial C^*}{\partial y^*}\frac{\partial T^*}{\partial y^*}\right)+\frac{D_T}{Tm}\left(\frac{\partial T^*}{\partial y^*}\right)^2\right] \quad ...(7)$$

By introducing non-dimensional variables,

$$P^*=\frac{\mu_f PU}{h},\ t^*=\frac{t}{\omega},\ T^*=T_0+\theta(T_1-T_0),\ u^*=uU,\ y^*=yh,\ x^*=xh,\ C^*=C_0+\phi(C_1-C_0) \quad .... (8)$$

where, ω is frequency, u, θ, ϕ represents the velocity, temperature and concentration in dimensionless form. Transforming the Eqs (2), (4) and (7) by using Eq. (8), we obtain

$$H^2\frac{\partial u}{\partial t}+R\frac{\partial u}{\partial y}=-\frac{\partial P}{\partial x}+\left(1+\frac{1}{\beta}\right)\left(\frac{\partial^2 u}{\partial y^2}\right)+\frac{Gr}{Re}\theta+\frac{Gc}{Re}\phi-\left(M^2+\frac{1}{Da}\right)u-FsReu^2 \quad ...(9)$$

$$H^2\frac{\partial\theta}{\partial t}+R\frac{\partial\theta}{\partial y}=\frac{1}{Pr}\left(1+\frac{4}{3}Rd\right)\frac{\partial^2\theta}{\partial y^2}+Nb\frac{\partial\theta}{\partial y}\frac{\partial\phi}{\partial y}+Nt\left(\frac{\partial\theta}{\partial y}\right)^2+\left(1+\frac{1}{\beta}\right)Ec\left(\frac{\partial u}{\partial y}\right)^2+M^2Ecu^2+Q\theta \quad ...(10)$$

$$LePrH^2\frac{\partial\phi}{\partial t}+LePrR\frac{\partial\phi}{\partial y}=\frac{\partial^2\phi}{\partial y^2}+\frac{Nt}{Nb}\frac{\partial^2\theta}{\partial y^2}-\gamma LePr\phi-K_1LePr. \quad ... (11)$$

where, $Fs=\frac{C_bh}{\sqrt{k}}$ (Forchheimer number), $H=\frac{h\sqrt{\omega}}{\sqrt{\nu_f}}$ (frequency parameter), $Pr=\frac{\nu_f}{\alpha}$ (Prandtl number), $Q=\frac{Q_0h^2}{(\rho C_p)_f\nu_f}$ (heat source/sink parameter), $Nt=\frac{\tau D_T(T_1-T_0)}{Tm\nu_f}$ (thermophoresis parameter), $Re=\frac{Uh}{\nu_f}$ (Reynolds number), ω (frequency), $Gc=\frac{g\beta_C^*(C_1-C_0)h^3}{\nu_f^2}$ (solutal

Grashof number), $Ec = \frac{U^2}{C_p(T_1 - T_0)}$ (Eckert number), $Rd = \frac{4\sigma^* T_0^3}{\kappa_f \chi}$ (radiation parameter), $Nb = \frac{\tau D_B (C_1 - C_0)}{\nu_f}$ (Brownian motion parameter), $\gamma = \frac{k_1 h^2}{\nu_f}$ (chemical reaction parameter), U (characteristic velocity), $K_1 = \frac{k_1 C_0 h^2}{\nu_f (C_1 - C_0)}$, $Le = \frac{\alpha}{D_B}$ (Lewis number), $\alpha = \frac{\kappa_f}{(\rho C_p)_f}$ (thermal diffusivity), $Da = \frac{k}{(\Phi h^2)}$ (Darcy number of the porous media), $Gr = \frac{g\beta_T^*(T_1 - T_0)h^3}{\nu_f^2}$ (Grashof number), $R = \frac{v_0 h}{\nu_f}$ (cross flow Reynolds number, $M = \frac{B_0 h\sqrt{\sigma_f}}{\sqrt{\mu_f}}$ (Hartmann number).

The transformed conditions are

$$u(0) = 0, \theta(0) = 0, \phi(0) = 0;\ u(1) = 0,\ \theta(1) = 1,\ \phi(1) = 1. \quad ...(12)$$

Method of solution

To get the solution of Eqs (9)-(11), a perturbation approach has been assumed in the form:

$$-\frac{\partial P}{\partial x} = A_0 + \varepsilon A_1 e^{it};\ u = u_0(y) + \varepsilon u_1(y)e^{it}, \theta = \theta_0(y) + \varepsilon\theta_1(y)e^{it}, \phi = \phi_0(y) + \varepsilon\phi_1(y)e^{it}. \quad ...(13)$$

and omitting higher orders.

Substitute Eq. (13) into Eqs. (9)-(11) and on comparing the coefficients of same powers of ε, we obtain

$$\left(1 + \frac{1}{\beta}\right)u_0'' - Ru_0' - \left(M^2 + \frac{1}{Da}\right)u_0 + A_0 + \frac{Gr}{Re}\theta_0 + \frac{Gc}{Re}\phi_0 - FsRe u_0^2 = 0 \quad \cdots(14)$$

$$\left(1 + \frac{1}{\beta}\right)u_1'' - Ru_1' - \left(M^2 + \frac{1}{Da} + iH^2\right)u_1 + A_1 + \frac{Gr}{Re}\theta_1 + \frac{Gc}{Re}\phi_1 - 2FsRe u_0 u_1 = 0 \quad \cdots(15)$$

$$\left(1 + \frac{4}{3}Rd\right)\theta_0'' - R\,\mathrm{Pr}\,\theta_0' + QPr\theta_0 + NbPr\theta_0'\phi_0' + NtPr(\theta_0')^2 + \left(1 + \frac{1}{\beta}\right)EcPr(u_0')^2 + M^2 EcPr u_0^2 = 0 \quad \cdots(16)$$

$$\left(1 + \frac{4}{3}Rd\right)\theta_1'' - R\,\mathrm{Pr}\,\theta_1' + (QPr - iH^2 Pr)\theta_1 + Nb(\theta_0'\phi_1' + \theta_1'\phi_0')Pr + 2NtPr\theta_0'\theta_1' + 2\left(1 + \frac{1}{\beta}\right)EcPru_0'u_1' + 2M^2 EcPru_0 u_1 = 0 \quad \cdots(17)$$

$$\phi_0'' - Le\,\mathrm{Pr}\,R\phi_0' - \gamma LePr\phi_0 + \left(\frac{Nt}{Nb}\right)\theta_0'' - K_1 LePr = 0 \quad \cdots(18)$$

$$\phi_1'' - Le\,\mathrm{Pr}\,R\phi_1' - LePr(iH^2 + \gamma)\phi_1 + \left(\frac{Nt}{Nb}\right)\theta_1'' = 0 \cdots(19)$$

The corresponding boundary conditions are

$$u_1(0) = 0,\ u_0(0) = 0, u_1(1) = 0,\ u_0(1) = 0;\ \theta_1(0) = 0,\ \theta_0(0) = 0,\ \theta_1(1) = 0,\ \theta_0(1) = 1;\ \phi_1(0) = 0,\ \phi_0(0) = 0,\ \phi_1(1) = 0,\ \phi_0(1) = 1. \quad \cdots(20)$$

Further, the non-dimensional rate of mass transfer (Sh), and heat transfer rate (Nu) at the channel boundaries can be obtained from

$$Nu = \left.\frac{d\theta}{dy}\right|_{y=0,1} \text{ and } Sh = \left.\frac{d\phi}{dy}\right|_{y=0,1} \quad ... (21)$$

Numerical analysis

With the use of the R-K 4th order method along with the Shooting technique, the numerical findings established to the coupled non-linear ODE's (14)-(19) and the associated conditions Eq. (20) are solved using the shooting method. The step size is fixed as 0.001 (i.e., $\Delta y = 0.001$) precision is static for the convergence criteria. The system of ODEs is changed into a collection of first-order ODEs. By using the equations, we can now define a new set of variables:

$$u_0 = \zeta_1, u_0' = \zeta_2, u_1 = \zeta_3, u_1' = \zeta_4,\ \theta_0 = \zeta_5, \theta_0' = \zeta_6, \theta_1 = \zeta_7, \theta_1' = \zeta_8, \phi_0 = \zeta_9, \phi_0' = \zeta_{10}, \phi_1 = \zeta_{11}, \phi_1' = \zeta_{12} \quad \cdots(22)$$

Putting Eq. (22) in Eqs (14)-(19) results in the simplified equations listed below:

$$\zeta_2' = \left(\frac{1}{1 + \frac{1}{\beta}}\right)\left\{\begin{array}{l} R\zeta_2 + \left(M^2 + \frac{1}{Da}\right)\zeta_1 - A_0 - \frac{Gr}{Re}\zeta_5 \\ -\frac{Gc}{Re}\zeta_9 + FsRe\zeta_1^2 \end{array}\right\} \quad \cdots(23)$$

$$\zeta_4' = \left(\frac{1}{1 + \frac{1}{\beta}}\right)\left\{\begin{array}{l} R\zeta_4 + \left(M^2 + \frac{1}{Da} + iH^2\right)\zeta_3 - A_1 \\ -\frac{Gr}{Re}\zeta_7 - \frac{Gc}{Re}\zeta_{11} + 2FsRe\zeta_1\zeta_3 \end{array}\right\} \quad \cdots(24)$$

$$\zeta_6^{'}=\left(\frac{1}{1+\frac{4}{3}Rd}\right)\left\{\begin{array}{l}R\,\mathrm{Pr}\,\zeta_6-QPr\zeta_5-NbPr\zeta_6\zeta_{10}-NtPr\zeta_6^{\,2}\\-\left(1+\frac{1}{\beta}\right)EcPr\zeta_2^{\,2}-M^2EcPr\zeta_1^{\,2}\end{array}\right\} \quad \cdots(25)$$

$$\zeta_8^{'}=\left(\frac{1}{1+\frac{4}{3}Rd}\right)\left\{\begin{array}{l}R\,\mathrm{Pr}\,\zeta_8-(QPr-iH^2Pr)\zeta_7-Nb(\zeta_6\zeta_{12}\\+\zeta_8\zeta_{10})Pr-2NtPr\zeta_6\zeta_8\\-2\left(1+\frac{1}{\beta}\right)EcPr\zeta_2\zeta_4-2M^2EcPr\zeta_1\zeta_3\end{array}\right\} \quad \cdots(26)$$

$$\zeta_{10}^{'}=\left\{Le\,\mathrm{Pr}\,R\zeta_{10}+\gamma LePr\zeta_9-\left(\frac{Nt}{Nb}\right)\zeta_6^{'}+K_1LePr\right\} \quad \cdots(27)$$

$$\zeta_{12}^{'}=\left\{Le\,\mathrm{Pr}\,R\zeta_{12}+LePr(iH^2+\gamma)\zeta_{11}-\left(\frac{Nt}{Nb}\right)\zeta_8^{'}\right\}\cdots(28)$$

with the boundary conditions

$$\zeta_1(0)=0,\zeta_3(0)=0,\zeta_5(0)=0,\zeta_7(0)=0,\zeta_9(0)=0,\zeta_{11}(0)=0;\zeta_1(1)=0,\zeta_3(1)=0,\zeta_5(1)=1,\zeta_7(1)=0,\zeta_9(1)=1,\zeta_{11}(1)=0. \quad \cdots(29)$$

Throughout the calculations, the considered parametric values are $Nt=0.2$, $Le=1$, $\gamma=1$, $K_1=0.001$, $Nb=0.2$, $\mathrm{Pr}=21$, $H=2$, $\beta=2$, $M=2$, $t=\pi/4$, $Gc=7$, $Gr=5$, $\mathrm{Re}=1$, $Fs=0.5$, $Da=0.5$, $\mathrm{R}=1$, $A_0=1$, $A_1=1$, $\varepsilon=0.001$, $Rd=2$, $Q=-0.5$, $Ec=0.4$, unless otherwise stated.

Results and Discussion

The influences of several relevant parameters on flow variables have been addressed in the current section with the aid of graphical results. The behaviour of Fs, Da, Gr, Gc, M, and β on the velocity profile is plotted in Figs 2(a) to 2(f). Fig. 2(a) depicts how the Forchheimer number impacts the velocity field. It is clear that u decreases when Fs rises. Fig. 2(b) depicts the impact of Da on u. Here, the velocity profile u increases by rising the porosity parameter. The impact of the Gr on the velocity field is depicted in Fig. 2(c). The outcome demonstrates that a rise in Grashof number causes an increase in the velocity field because buoyancy forces increase. Analysing the effect of various solutal Grashof number values on u yields a similar result (Fig. 2(d)). Fig. 2(e) elucidates the effect of M on the velocity field. The applied magnetic field produced a drag force opposing the flow direction. It seems that the larger values of M lead to a fall in velocity. The Casson fluid parameter impact on the Casson fluid flow velocity is depicted in Fig. 2(f). Physical relationships between the Casson fluid parameter and fluid viscosity cause the fluid viscosity to rise as the Casson fluid parameter rises. Increased viscosity results in decreased velocity.

Fig. 3(a) depicts the variations in temperature distribution with Nb. It is obvious that rising Nb will significantly rise the fluid's temperature. Fig. 3(b) describes the variation of unsteady temperature distributions for various values of Nb. Further, it is noted that the unsteady temperature fluctuates with rising Nb, and the maximum is located closer to the walls. By changing Nt on θ, similar behaviour can be observed (see Figs 4(a) and 4(b)). As the Brownian motion strengthens, this leads to effective movement of nanoparticles from the walls to the fluid. Because of this reason, the dimensionless temperature θ increases with an increase in Nb. It may be noted that the parameters Nb and Nt characterize the strengths of Brownian motion and thermophoresis effects. The larger values of Nb and Nt, the larger the strength of the corresponding effects. Thus Nb and Nt can take any value in the range of $0 \le Nb\,;\, Nt < 1$. Fig. 5(a) depicts the impact of Rd on θ. Here, the temperature profile θ increases by increasing Rd. Fig. 5(b) illustrates how the unsteady temperature oscillates with rising Rd and shifts its maximum to be close to the walls. Fig. 6 depicts how influences unsteady velocity and temperature fields. It is clear that the unsteady temperature and velocity fields oscillate as they rise.

The impact on concentration distribution is seen in Fig. 7(a). With a rise in γ, it is seen that the distributions of nanoparticle concentrations decrease. The largest unsteady nanoparticle concentration is found closer to the walls and changes with increased γ (see Fig. 7(b)).Similar results are obtained when different Lewis number values are examined in relation to concentration distribution (see Figs 8(a) and 8(b)).

Table 1 displays the steady and unsteady Nusselt number distributions (Nu_s and Nu_t) at the left wall for various values of Rd, Q, M, Ec, Nb, and Nt. The steady and unsteady heat transfer rates are said to decrease by rising the values of the Brownian motion parameter and Hartmann number, while the increasing heat source or sink parameter, radiation parameter, Eckert number, and thermophoresis parameter exhibit rising behaviour. The steady and unsteady Sherwood number distributions (Sh_s and Sh_t) at the left wall

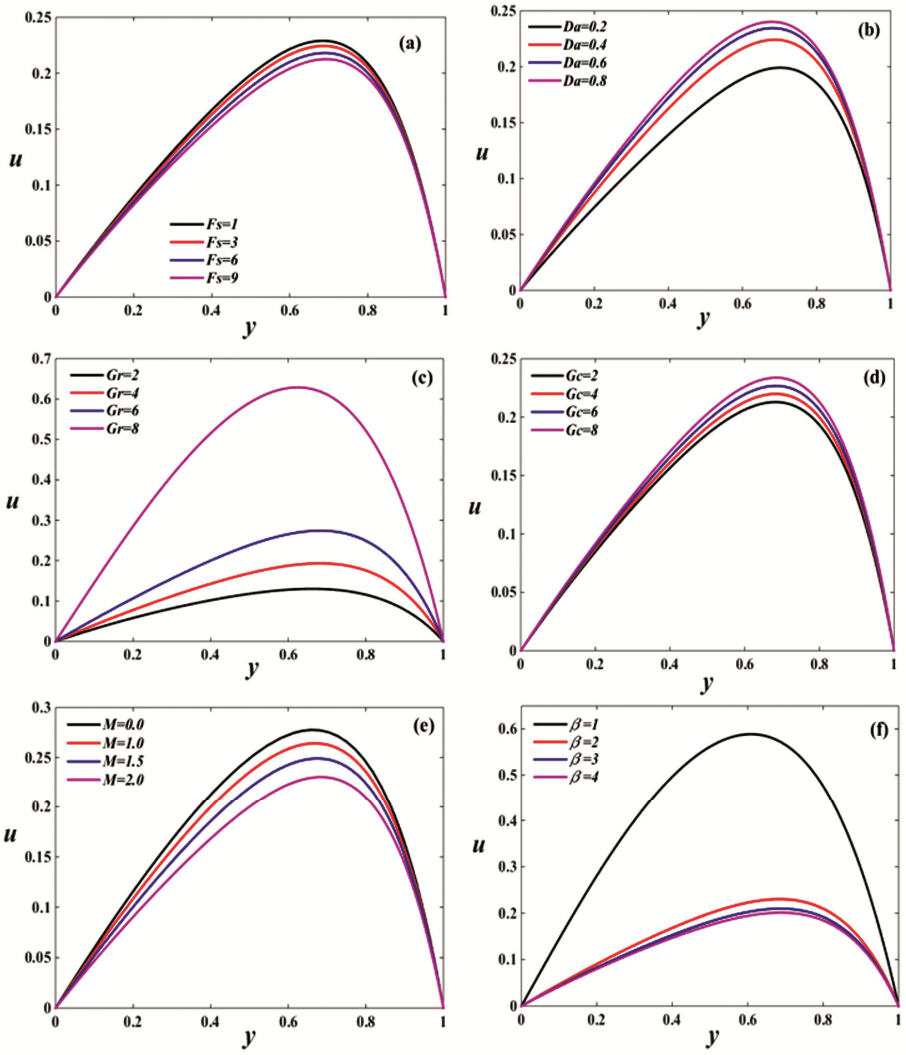

Fig. 2 — Velocity distribution under the (a) influence of Fs, (b) influence of Da, (c) influence of Gr,(d) influence of Gc, (e) influence of M and (f) influence of β.

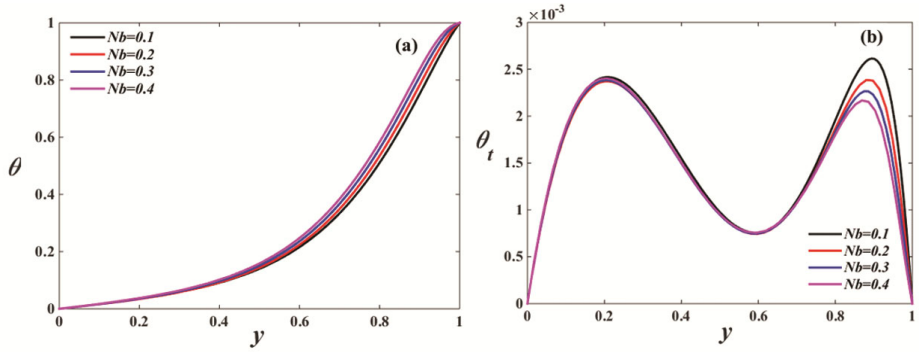

Fig. 3 — Influence of Nb on temperature distribution

for different values of β, M, Le, γ, Nt, and Nb are presented in Table 2. According to Table 2, the higher values of the chemical reaction, Hartmann number, and Casson fluid parameter result in an increase in both the steady and unsteady mass transfer rate distributions. One can notice that for a given

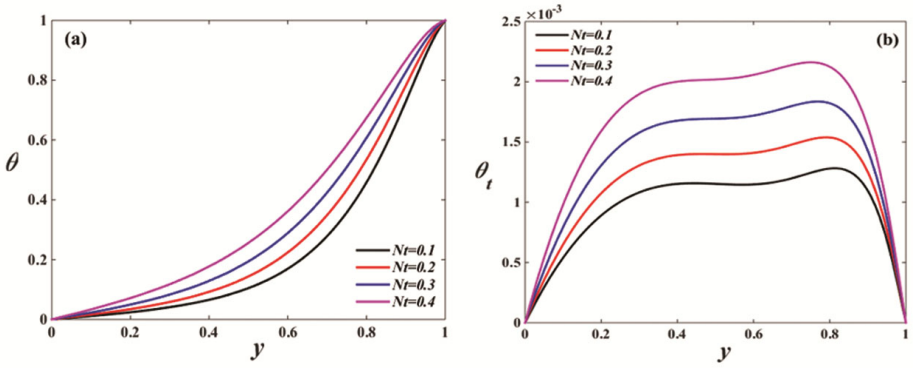

Fig. 4 — Influence of Nt on temperature distribution

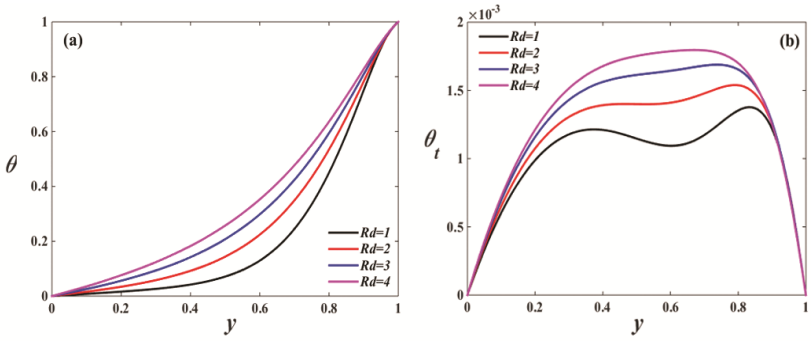

Fig. 5 — Influence of Rd on temperature distribution

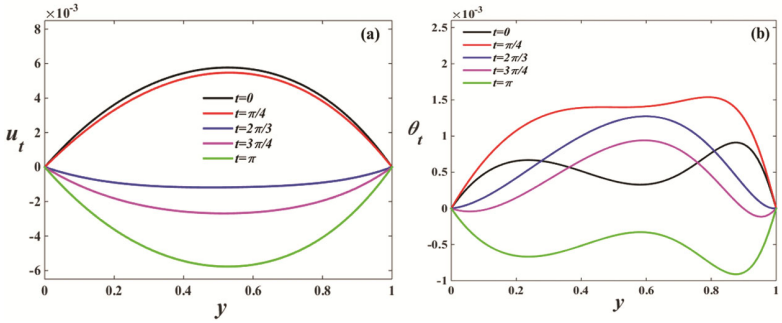

Fig. 6 — Influence of t on unsteady velocity and temperature distributions

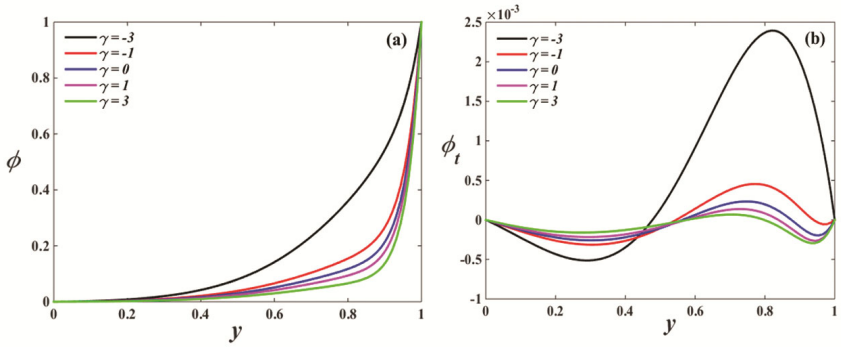

Fig. 7 — Influence of γ on concentration distribution

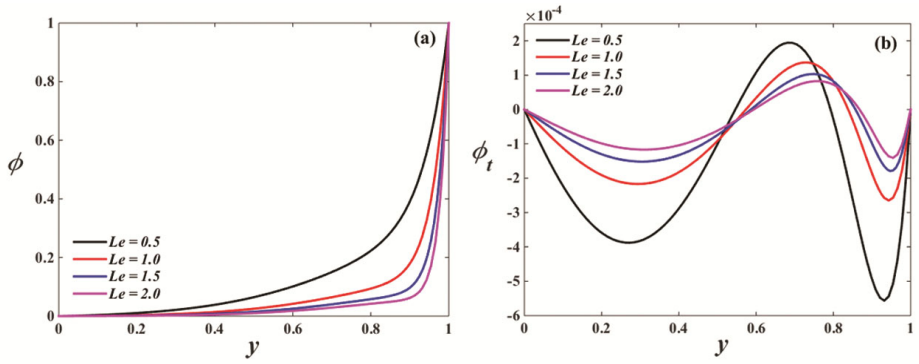

Fig. 8 — Influence of Le on concentration distribution

Table 1 — Distributions of Nu_s (θ_0') and Nu_t ($\varepsilon\theta_1'\exp(it)$) for different values of Rd, Q, Ec, M, Nb, and Nt at $Le = 1$, $\gamma = 1$, $K_1 = 0.001$, $\Pr = 21$, $H = 2$, $\beta = 2$, $t = \pi/4$, $Gc = 7$, $Gr = 5$, $\mathrm{Re} = 1$, $Fs = 0.5$, $Da = 0.5$, $\mathrm{R} = 1$, $A_0 = 1$, $A_1 = 1$, $\varepsilon = 0.001$

Rd	Q	Ec	M	Nb	Nt	Nu_s	Nu_t
1						0.084224	0.000716
2						0.152704	0.000772
3						0.246218	0.000821
4						0.338486	0.000847
	-0.3					0.173144	0.000819
	-0.1					0.199512	0.000874
	0.1					0.234989	0.000941
	0.3					3.137998	0.003146
		0.1				0.056169	0.000159
		0.2				0.083344	0.000337
		0.3				0.115032	0.000540
		0.4				0.152704	0.000772
			0			0.205706	0.001110
			1			0.189731	0.001008
			1.5			0.172536	0.000898
			2			0.152704	0.000772
				0.1		0.157856	0.000796
				0.2		0.152704	0.000772
				0.3		0.157731	0.000782
				0.4		0.164455	0.000799
					0.1	0.108297	0.000643
					0.2	0.152704	0.000772
					0.3	0.219503	0.000946
					0.4	0.320813	0.001181

Table 2 — Distributions of Sh_s (ϕ_0') and Sh_t ($\varepsilon\phi_1'\exp(it)$) for different values of β, M, Nb, Nt, γ and Le at $K_1 = 0.001$, $\Pr = 21$, $H = 2$, $t = \pi/4$, $Gc = 7$, $Gr = 5$, $\mathrm{Re} = 1$, $Fs = 0.5$, $Da = 0.5$, $\mathrm{R} = 1$, $A_0 = 1$, $A_1 = 1$, $\varepsilon = 0.001$, $Rd = 2$, $Q = -0.5$, $Ec = 0.4$

β	M	Nb	Nt	γ	Le	Sh_s	Sh_t
1						-0.139034	-0.000688
2						0.005432	-0.000119
3						0.006468	-0.000101
4						0.006819	-0.000094

(contd.)

Table 2 — Distributions of Sh_s (ϕ_0') and Sh_t ($\varepsilon\phi_1'\exp(it)$) for different values of β, M, Nb, Nt, γ and Le at $K_1 = 0.001$, $\Pr = 21$, $H = 2$, $t = \pi/4$, $Gc = 7$, $Gr = 5$, $\mathrm{Re} = 1$, $Fs = 0.5$, $Da = 0.5$, $\mathrm{R} = 1$, $A_0 = 1$, $A_1 = 1$, $\varepsilon = 0.001$, $Rd = 2$, $Q = -0.5$, $Ec = 0.4$ (*contd.*)

β	M	Nb	Nt	γ	Le	Sh_s	Sh_t
	0					-0.004629	-0.000203
	1					-0.001314	-0.000176
	1.5					0.001992	-0.000149
	2					0.005432	-0.000119
		0.1				0.009872	-0.000242
		0.2				0.005432	-0.000119
		0.3				0.003832	-0.000080
		0.4				0.002979	-0.000061
			0.1			0.000832	-0.000050
			0.2			0.005432	-0.000119
			0.3			0.014021	-0.000219
			0.4			0.026102	-0.000381
				-3		0.012964	-0.000201
				-1		0.007327	-0.000139
				1		0.005432	-0.000119
				3		0.004423	-0.000106
					0.5	0.025686	-0.000250
					1	0.005432	-0.000119
					1.5	0.001935	-0.000076
					2	0.000723	-0.000056

Table 3 — Comparison of the current results to those of Radhakrishnamacharya and Maiti[17] and to the outcomes of ND Solve for $\left(\theta_0'\right)_{y=0}$ and $\left(\theta_0'\right)_{y=1}$ for the Newtonian fluid in the absence of nanoparticle concentration, thermophoresis parameter, Brownian motion parameter, Grashof number, solutal Grashof number, heat source/sink parameter, thermal radiation, applied magnetic field, and Darcian and non-Darcian porous medium

Ec	$\left(\theta_0'\right)_{y=0}$			$\left(\theta_0'\right)_{y=1}$		
	Radhakrishnamacharya & Maiti[17]	Present results	NDSolve	Radhakrishnamacharya & Maiti[17]	Present results	NDSolve
1	0.233	0.2315	0.2315	-1.440	-1.4398	-1.4410
2	0.308	0.3058	0.3058	-3.199	-3.1997	-3.1989
5	0.531	0.5288	0.5288	-8.993	-8.9937	-8.9999

increase in Nb, Sh_s decreases and Sh_t increases at the left wall. By changing Le, the identical behaviour can be observed. One can infer that for a given rise in Nt, Sh_s increases and Sh_t decreases at $y = 0$. Additionally, the results of Radhakrishnamacharya and Maiti[17], which are shown in Table 3, are in good accord with the findings of the current study when taken as a limiting case.

Conclusion

In this study, MHD pulsatile flow of electrically conducting Casson nanofluid in a vertical porous channel in the presence of viscous dissipation, and Ohmic heating has been analysed using Buongiorno model. Buongiorno nanofluid model is focused to view the Brownian movement and thermophoretic influences. The effect of chemical reaction parameter is taken into the account. The present work is significant in the field of nano-drug delivery, dynamics of physiological fluids, and biomedicines. Particularly the pulsatile flow in a porous channel is important in the dialysis of blood in artificial kidneys. The influence of Ohmic heating and thermal radiation on chemically reactive pulsatile flow of Casson nanofluid in a vertical porous channel embedded in non-Darcy porous medium is the novelty of the present study. The governing partial differential equations are changed into system of ordinary differential equations by employing the perturbation method, then solved by adopting fourth-order Runge–Kutta method along with the aid of shooting

technique. The following are the key conclusions from this investigation:

(i) The velocity is decreased by a rise in the Casson nanofluid parameter & Forchheimer number, whereas a rise in the Grashof number increases the velocity.

(ii) As the parameters of the Lewis number and chemical reaction rise, then a noparticle concentration distribution decreases.

(iii) Heat transfer rate is an enhancing function of Eckert number and radiation parameters while it is a lowering function of Brownian motion parameter.

(iv) By taking $M = 0$, as a limiting case, the results corresponding to the problem for the hydrodynamic case can be captured.

(v) The results of Radhakrishnamacharya and Maiti[17] for the case of Newtonian fluid can be captured from the present analysis by taking $Nb = Nt = Q = Rd = M = Gr = Gc = Da = Fs = 0$ in the absence of nanoparticle concentration.

References

1 Choi S U S & Eastman J A, Enhancing thermal conductivity of fluids with nanoparticles, *Am Soc Mech Eng Fluids Eng Div FED*, 231 (1995) 99.

2 Hatami M, Hatami J & Ganji D D, Computer simulation of MHD blood conveying gold nanoparticles as a third grade non-Newtonian nanofluid in a hollow porous vessel, *Comput Meth Prog Biomed*, 113 (2014) 632.

3 Nield D A & Kuznetsov A V, Forced convection in a parallel-plate channel occupied by a nanofluid or a porous medium saturated by a nanofluid, *Int J Heat Mass Transfer*, 70 (2014) 430.

4 Malvandi A & Ganji D D, Brownian motion and thermophoresis effects on slip flow of alumina/water nanofluid inside a circular microchannel in the presence of a magnetic field, *Int J Therm Sci*, 84 (2014) 196.

5 Azimi M & Riazi R, Analytical solution of unsteady GO-water nanofluid flow and heat transfer between two parallel moving plates, *Indian J Chem Technol*, 23 (2016) 47.

6 Sheikholeslami M & Chamkha A J, Influence of Lorentz forces on nanofluid forced convection considering Marangoni convection, *J Mol Liq*, 225 (2017) 750.

7 Kumar R, Kumar R, Vajravelu K & Sheikholeslami M, Three dimensional stagnation flow of Casson nanofluid through Darcy-Forchheimer space: A reduction to Blasius/Sakiadis flow, *Chin J Phys*, 68 (2020) 874.

8 Waqas H, Naeem H, Manzoor U, Sivasankaran S, Alharbi A A, Alshomrani, A S & Muhammad T, Impact of electro-magneto-hydrodynamics in radiative flow of nanofluids between two rotating plates, *Alex Eng J*, 61 (2022) 10307.

9 Chaudhary S, Analysis of Cu - water nanofluid flow with different particle shapes over an isothermal moving plate, *Indian J Chem Technol*, 29 (2022) 311.

10 Srinivas S, Kumar C K, Badeti S & Reddy A S, MHD flow of Casson nanofluid over an inclined porous stretching surface, *Recent Advances in Applied Mathematics and Applications to the Dynamics of Fluid Flows* (Springer Nature, Singapore) (2023) 155.

11 Buongiorno J, Convective transport in nanofluids, *J Heat Mass Transfer*, 128 (2006) 240.

12 Ghasemi S E, Vatani M, Hatami M & Ganji D D, Analytical and numerical investigation of nanoparticle effect on peristaltic fluid flow in drug delivery systems, *J Mol Liq*, 215 (2016) 88.

13 Ghadikolaei S S, Hosseinzadeh K, Ganji D D & Jafari B, Nonlinear thermal radiation effect on magneto Casson nanofluid flow with Joule heating effect over an inclined porous stretching sheet, *Case Stud Therm Eng*, 12 (2018) 176.

14 Das S, Ali A, Jana R N & Makinde O D, EDL impact on mixed magneto-convection in a vertical channel using ternary hybrid nanofluid, *Chem Eng J Adv*, 12 (2022) 100412.

15 Farooq U, Waqas H, Alhazmi S E, Alhushaybari A, Imran M, Sadat R, Muhammad T & Ali M R, Numerical treatment of Casson nanofluid Bioconvectional flow with heat transfer due to stretching cylinder/plate: Variable physical properties, *Arab J Chem*, 16 (2023) 104589.

16 Wang C Y, Pulsatile Flow in a Porous Channel, *J Appl Mech Trans ASME*, 38 (1971) 553.

17 Radhakrishnamacharya G & Maiti M K, Heat transfer to pulsatile flow in a porous channel, *J Heat Mass Transfer*, 20 (1977) 171.

18 Bestman A R, Pulsatile flow in heated porous channel, *Int J Heat Mass Transfer*, 25 (1982) 675.

19 Srinivas S, Kumar C K & Reddy A S, Pulsating flow of Casson fluid in a porous channelwith thermal radiation, chemical reaction and appliedmagnetic field, *Nonlinear Anal Model Control*, 23 (2018) 213.

20 Cheng Z, Jelly T O, Illingworth S J, Marusic I & Ooi A S H, Forcing frequency effects on turbulence dynamics in pulsatile pipe flow, *Int J Heat Fluid Flow*, 82 (2020) 108538.

21 Bianco V, Trubatch A D, Wei H & Yecko P, Quantifying volume loss of a magnetically localized ferrofluid bolus in pulsatile pipe flow, *J Magn Magn Mater*, 524 (2021) 167595.

22 Datta N, Dalal D C & Mishra S K, Unsteady heat transfer to pulsatile flow of a dusty viscous incompressible fluid in a channel, *Int J Heat Mass Transfer*, 36 (1993) 1783.

23 Rana J & Murthy P V S N, Solute dispersion in pulsatile Casson fluid flow in a tube with wall absorption, *J Fluid Mech*, 793 (2016) 877.

24 Shit G C, Maiti S, Roy M & Misra J C, Pulsatile flow and heat transfer of blood in an overlapping vibrating atherosclerotic artery: A numerical study, *Math Comp Simul*, 166 (2019) 432.

25 Kumar C K, Srinivas S & Reddy A S, MHD Pulsating Flow of Casson Nanofluid in a Vertical Porous Space with Thermal Radiation and Joule Heating, *J Mech*, 36 (2020) 535.

26 Vasu B, Dubey A, Bég O A & Gorla R S R, Micropolar pulsatile blood flow conveying nanoparticles in a stenotic tapered artery: Non-Newtonian pharmacodynamic simulation, *Comput Biol Med*, 126 (2020) 104025.

27 Kumar C K & Srinivas S, Pulsating hydromagnetic flow of Casson fluidin a vertical channel filled with non-Darcianporous medium, *Heat Transfer,* 50 (2021) 5225.

28 Ali A, Fatima A, Bukhari Z, Farooq H & Abbas Z, Non-Newtonian Casson pulsatile fluid flow influenced by Lorentz force in a porous channel with multiple constrictions: A numerical study, *Korea-Aust Rheol J*, 33 (2021) 79.
29 Govindarajulu K & Reddy A S, Magnetohydrodynamic pulsatile flow of third grade hybrid nanofluid in a porous channel with Ohmic heating and thermal radiation effects, *Phys Fluids*, 34 (2022) 013105.
30 Wang X, Qiao Y, Qi H & Xu H, Numerical study of pulsatile non-Newtonian blood flow and heat transfer in small vessels under a magnetic field, *Int Commun Heat Mass Transfer*, 133 (2022) 105930.
31 Srinivas S, Kumar C K & Reddy A S, Dufour and Soret effects on pulsatile hydromagnetic flow of Casson fluid in a vertical non-Darcian porous space, *Nonlinear Anal Model Control*, 27 (2022) 669.
32 Bridges C & Rajagopal K R, Pulsatile Flow of a Chemically-Reacting Nonlinear Fluid, *Comput Math Appl*, 52 (2006) 1131.
33 Vajravelu K, Prasad K V & Rao N S P, Diffusion of a chemically reactive species of a power-law fluid past a stretching surface, *Comput Math Appl*, 62 (2011) 93.
34 Hayat T, Yasmin H, Asghar S & Hendi A A, Slip effects on peristaltic transport in an inclined channel with mass transfer and chemical reaction, *Appl Bionics Biomech*, 10 (2013) 41.
35 Chand K, Singh K D & Sharma S, Combined effect of chemical reaction and radiation on heat and mass transfer in oscillatory MHD flow of viscoelastic fluid through vertical channel, *Res J Sci Technol*, 5 (2013) 77.
36 Kumar C K & Srinivas S, Simultaneous effects of thermal radiation and chemical reaction on hydromagnetic pulsatile flow of a Casson fluid in a porous space, *Eng Transfer*, 65 (2017) 461.
37 Alzahrani A K, Abbas Z & Ullah M Z, Chemically reactive two-phase flow of viscous-Casson fluids in a rotating channel, *Alex Eng J*, 62 (2023) 403.
38 Rauf A, Siddiq M K, Abbasi F M, Meraj M A, Ashraf M & Shehzad S A, Influence of convective conditions on three dimensional mixed convective hydromagnetic boundary layer flow of Casson nanofluid, *J Magn Magn Mater*, 416 (2016) 200.
39 Raju C S K, Sandeep N, Sugunamma V, Babu M J & Reddy J V R, Heat and mass transfer in magnetohydrodynamic Casson fluid over an exponentially permeable stretching surface, *Eng Sci Technol Int J*, 19 (2016) 45.
40 Swarnalathamma B V, Babu D M P & Krishna M V, Combined impacts of radiation absorption and chemically reacting on MHD free convective casson fluid flow past an infinite vertical inclined porous plate, *J Comput Math Data Sci*, 5 (2022) 100069.
41 Asogwa K K, Goud B S, Reddy Y D & Ibe A A, Suction effect on the dynamics of EMHD Casson nanofluid over an induced stagnation point flow of stretchable electromagnetic plate with radiation and chemical reaction, *Res Eng*, 15 (2022) 100518.
42 Yousef N S, Megahed A M, Ghoneim N I, Elsafi M & Fares E, Chemical reaction impact on MHD dissipative Casson-Williamson nanofluid flow over a slippery stretching sheet through porous medium, *Alex Eng J*, 61 (2022) 10161.
43 Devi M P & Srinivas S, Two layered immiscible flow of viscoelastic liquid in a vertical porous channel with Hall current, thermal radiation and chemical reaction, *Int Commun Heat Mass Transfer*, 142 (2023) 106612.
44 Srinivas S, Challa K K, Badeti S & Kumar P B, Pulsatile powell-eyring nanofluid flow in a channel with inclined magnetic field and chemical reaction, *Eng Trans*, 71 (2023) 519.